UPPSALA
UNIVERSITET

Uppsala University
Department of Physics and Astronomy
Materials Physics Division

Research Project Report

Tunable perpendicular anisotropy in δ-doped Co/Fe-V superlattices

Pascal Bliem

Supervisors:
Heikki Palonen
Björgvin Hjörvarsson

Uppsala, February 2017

Abstract

In this work, we investigate the effect of varying Co δ-layer density on anisotropy in $Co/Fe_{31}V_{69}$ superlattices. Samples were grown epitaxially on MgO via direct-current magnetron sputtering and characterised by x-ray diffraction, x-ray reflectivity, and longitudinal magneto-optical Kerr effect measurements. Superlattices with one monolayer of Co per repetition exhibit excellent coherency and low uncorrelated interface roughness. Addition of Co layers reduces the temperature of zero in-plane magnetisation, indicating an out-of-plane canting angle of the magnetic moment. This perpendicular anisotropy originates from Co interfaces and is in competition with the shape anisotropy, which in turn, depends on the total magnetic moment of the film. We conclude that the degree of canting is tunable by temperature, Co layer density, and composition of the Fe-V alloy. An elevation of the total magnetic moment by higher Fe concentration or lower temperature increases the in-plane projection of the moment, whereas additional interfaces increase its out-of-plane projection.

Contents

1. Introduction

Magnetic thin films have led technological progress and miniaturisation for the last decades, being at the core of numerous applications in magnetic recording, data storage, and magneto-electronic devices. Different from their bulk counterparts, reduced symmetry and the relevance of surfaces and interfaces raise opportunities and challenges for potential applications. One of these challenges, which becomes more pronounced with decreasing size, is controlling the direction of magnetisation. However, a precise control of the magnetic moment is essential for reliable magnetic switching and data storage [1].

In ultra-thin films, the magnetic ordering temperature, T_c, is reduced, scaling with the film thickness, and can even approach zero in the monolayer (ML) limit [2]. Due to long-range magnetic interactions, the spatial region that is influenced by a surface or interface can be of considerable extend. Thus, very thin layers will effectively consist of merged surface or interface regions [3]. Naturally, this points interest on the effects that different materials have on each other, e.g., when sharing interfaces in layered structures. One relevant phenomenon, known as the magnetic proximity effect, describes how interface exchange coupling of a ferro- and a paramagnetic material can induce magnetisation in the latter [4]. Hybridisation of electronic states can create new magnetic states at the interface, which convey the proximity magnetisation over a certain range [5, 6]. This effect can even influence the T_c of the constituent materials [7]. In recent unpublished work of this group on Fe/Fe-V superlattices a new concept, the double proximity effect, has been introduced. This concept embraces the tuning of ferromagnetic behaviour by combining magnetic proximity and finite-size effects. Varying the spacing of Fe monolayers embedded in an Fe-V alloy allows to examine proximity induced magnetic ordering and interlayer coupling in these finite-size structures. In that study, the combination of two presumably paramagnetic components resulted in an overall ferromagnetic structure with enhanced T_c.

Another highly relevant property for applications is magnetic anisotropy. Magneto-crystalline anisotropy is caused by electrostatic interaction of orbitals with the crystal-field that stabilises orbitals along certain crystallographic directions. By spin-orbit coupling, the magnetic moment is then aligned in these particular directions. In addition, the demagnetising field in a thin film tends to force the direction of magnetisation into the thin film plane [1]. Nonetheless, a perpendicular magnetisation can often be desirable, for example in magnetic data storage, where it allows for a much higher storage density. Potential sources for an out-of-plane anisotropy are surfaces or interfaces in layered structures [8]. A particularly interesting candidate for such structures is Co, since it does not only have the highest T_c of all elements, but it is also known to promote perpendicular interface anisotropy. This behaviour is mostly observed in multilayers consisting of Co and a paramagnetic transition metal, such as Pd [9–15], Pt [10, 13], and Au [13, 16, 17], but also with magnetically ordered elements such as Cr [18], and Ni [19–22]. In these studies, the layers do either not form a single crystal lattice, or it is not clear if they do since no diffraction data is shown from which the crystal quality could be assessed. However, the extreme sensitivity of magnetic properties with respect to structure favours the use of fully coherent crystal lattices as a basis for addressing fundamental questions about magnetism. We, therefore, restrict our considerations to systems that can be grown with fully coherent crystal structure to avoid complications regarding the interpretation of magnetic behaviour.

Superlattices, delta-doped with Co, represent a material system which is excellently suitable for studying the magnetic double proximity effect in conjunction with anisotropy. In the following, we will present structural and magnetic characterisation of Co/Fe-V superlattices with varying Co layer density, accompanied by a discussion about the origins of different contributions to the magnetic anisotropy. We will show that anisotropy can be tuned with several parameters so that the direction of magnetisation can be continuously varied from in-plane to out-of-plane. In the end, we will give an outlook on how to address the questions that were left open in this study.

2. Methods

2.1 Growth

The samples synthesised in this study are superlattices and multilayers of $Co_n/(Fe_{31}V_{69})_m$ (where subscripts denote the number of monolayers (ML) with n=(1,2), m=(10, 15, 20, 30, 75)) as well as reference samples of the random $Fe_{31}V_{69}$ alloy. Every stack began with an Fe-V layer and was finished with an additional Fe-V layer to ensure identical boundary conditions for all Co layers. A schematic representation of the samples is shown in Figure 2.1 and an overview of all samples is given later on in Table 3.1. Note that the samples with m=75 only contain one Co repetition. All films (except relaxed Fe-V) were deposited on polished MgO(001) single crystals (10*10*1 mm) by direct current (DC) magnetron sputtering. The substrates were annealed at 1000° C for 10 minutes in ultra high vacuum (UHV) prior to deposition. All samples were co-sputtered from elemental Fe(99.95%), V(99.95%), Co(99.95%) 50.8 mm targets and capped at room temperature with a Pd layer (ca. 96 Å for n=1 and 48 Å for n=2). To enable two-dimensional growth and prevent

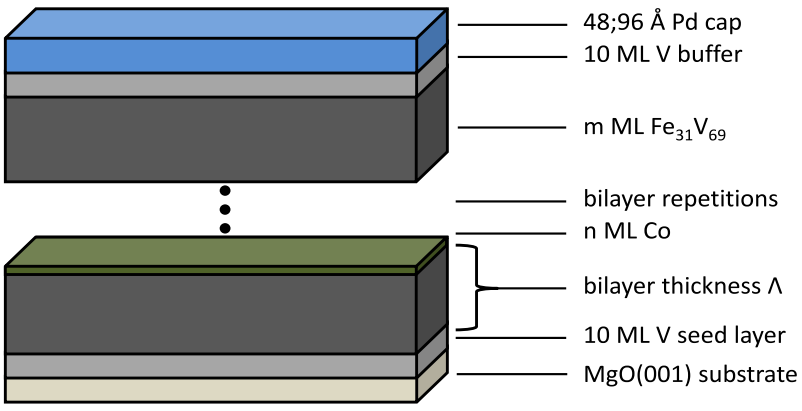

Figure 2.1: *A schematic representation of the samples. The dashed section represents the repetition of Co/Fe-V bilayers.*

a reaction of Fe with Pd, 10 ML of V were used as seeding and buffer layers between substrate and film, as well as film and cap. The films were grown at a temperature of 388° C, an Ar(99.99%) working pressure of 2 mTorr and a flow of 3 sccm. The background pressure was around $8x10^{-10}$ Torr. All relevant growth rates were calibrated via X-ray reflectivity (XRR) and kept at 0.199 Å/s for Co, 0.280 Å/s for V, 0.375 Å/s for Fe-V, and 0.719 Å/s for Pd. Together with shutters operating within an uncertainty of ±0.1 s, this allowed for a precise layer thickness control.

2.2 Characterisation

2.2.1 X-ray reflectivity

X-ray reflectivity (XRR) was performed on a Panalytical X'Pert MRD system using Cu K_α radiation and a proportional detector. A resolution of approximately 0.015° was achieved with a 0.09 mm divergence slit, Göbel mirror, 0.04 rad soller, and 10 mm mask (to avoid over-illumination of the sample in the transverse direction) in the incident beam path, and 0.09° parallel plate collimator with a selection slit in the exiting beam path. Sample height, ω-offset and ψ-offset were aligned in the direct beam and the total reflection. XRR scans were measured over a range of 2Θ = 0.1-10° with a step size of 0.02°. To account for a proper treatment of the background, scans were also taken with ω-offsets of ±0.05° and the average was subtracted from the main scan. The data was fitted with the GenX [23] code by simulating the XRR pattern resulting from a model of the samples, corresponding to the structure shown earlier in Figure 2.1. In this model, the thickness of Co/Fe-V bilayers (instead of individual layer thicknesses) was fitted and the interface roughnesses within the Co/Fe-V stack were constrained to the same value. Upper and lower errors were provided by GenX, using a logarithmic figure of merit, and the larger one is reported as standard error here.

2.2.2 X-ray diffraction

X-ray diffraction (XRD) was performed on a Panalytical X'Pert MRD system using Cu $K_{\alpha 1}$ radiation and a proportional detector. A resolution of approximately 0.008° was

achieved with a 1.4 mm (0.09 mm for alignment) divergence slit and hybrid mirror-monochromator in the incident beam path, and another Göbel mirror, 0.1 mm slit, and 0.04 rad soller in the exiting beam path. The sample height was aligned in the direct beam, while ω-offset and ψ-offset were aligned with respect to the lattice planes at the corresponding Bragg angle. XRD diffractograms and rocking curves were measured with a step size of 0.01° and 0.005°, respectively. Features in the diffractograms were fitted with Gaussian functions using the Levenberg-Marquardt method [24, 25], as implemented in the Fityk code [26], given the intensity square-root as weight. Propagating uncertainties in angle from instrumental resolution and fit, the standard error was calculated according to $\sigma = (\sum_i (\frac{\partial f(x)}{\partial x_i} \Delta x_i)^2)^{1/2}$ [27].

2.2.3 Magneto-optical Kerr effect measurements

The temperature-dependent magnetisation was measured using the magneto-optical Kerr effect (MOKE). Measurements were performed in a longitudinal-geometry setup with an optical cryostat cooled by liquid helium, a high-power diode laser (λ= 660 nm, P = 6 mW), a photo-diode detector, and two cross-polarisers. One of the polarisers is acting as an analyser set off by 2° from total extinction, which was chosen to ensure a good signal to noise ratio while staying in safe distance from total extinction. A pair of Helmholtz coils generated a 5 Hz alternating magnetic field with an amplitude of 7 mT. The cryostat was shielded against stray fields by three layers of μ-metal. Hysteresis loops were recorded in 1 K steps as an average over 500 loops with a sampling frequency of 50 kHz. Magnetisation vs. temperature data was fitted with power law functions, using the same method as for XRD, given the standard deviation of the averaged data as weight. Errors reported here are the parameter uncertainties from the fit.

3. Results and discussion

3.1 Structural properties

The magnetic behaviour of materials has a strong dependence on their structure. For instance, properties such as the magneto-crystalline anisotropy are determined by the type, coordination, and spacing of atoms in a solid [1]. It is therefore essential to carefully investigate the sample's structure to provide a well-founded basis for the discussion of magnetic properties.

To examine the crystal structure of the samples, we recorded high-resolution diffractograms and rocking curves around the (002) peak of the bcc lattices. It should

Table 3.1: *An overview of all samples investigated in this study. The columns display the number of bilayer repetitions, the total thickness D without buffer and cap layers, the bilayer thickness Λ, and the out-of-plane lattice parameter c.*

Sample	Repetitions	D (Å)	Λ (Å)	c (Å)
1-10	12	203(2)	15.7(1)	2.9375(7)
1-15	8	206(1)	23.1(2)	2.9179(7)
1-20	6	213(2)	30.6(3)	2.9362(7)
1-30	4	220(1)	44.2(2)	2.9155(7)
1-75	1	218(1)	109.5(3)	2.9248(7)
2-10	8	125(1)	16.0(2)	
2-30	4	225(2)	45.7(4)	
2-75	1	218(2)	110.5(9)	
Fe-V reference		217(1)		2.9205(7)
Fe-V relaxed*				2.922(1)

*Ca. 150 nm thick polycrystalline film grown on thermally oxidised Si.

be noted that the cubic lattice is actually tetragonally distorted, due to epitaxial growth on MgO with an in-plane lattice parameter of a=2.981 Å [28]. The out-of-plane lattice parameters in Table 3.1 do not show a Poisson response to a tetragonal distortion. The full width at half maximum (FWHM) of the films' rocking curves falls in the range of 0.03-0.11° and is proportional to the FWHM of the substrate rocking curves. This correlation masks any influence of films' degree of relaxation on the rocking curve width. The diffractograms are shown in Figure 3.1 b) and d) for the films with one and two ML Co per bilayer, respectively. Several distinctive features are visible in these scans; one of them being the Laue oscillations (also referred to as total thickness oscillations), which are distributed around the main peak, especially pronounced close to the main peak. The strong intensity of these oscillations in Figure 3.1 b) is an indication for a very good coherency of the single crystal lattice, resulting from well defined epitaxial growth and a low concentration of defects, such as misfit dislocations. Another feature which is clearly visible at higher angles is the occurrence of satellite peaks originating from the bilayer repetition. Their presence confirms a constant bilayer period Λ, which is related to the satellite distance ΔQ in momentum space by $\Lambda = 2\pi/\Delta Q$ [29]. The out-of-plane lattice parameters, c, of the n=1 series are given in Table 3.1. Dashed drop-lines in Figure 3.1 b) are used to emphasise that the main peak positions group around two values; the 1-10 and 1-20 samples residing at higher out-of-plane lattice spacing than 1-15 and 1-30, with 1-75 somewhat in between. With varying Co layer density, a monotonic shift of the measured (average) lattice parameter would be expected, assuming that the spacing between Co and Fe-V atomic planes at the interfaces differs from the one within the Fe-V alloy layers. The c values measured here, however, do not shift monotonically at all. This reveals that the variation of strain states in the different superlattices is rather complicated.

In Figure 3.1 d) the previously mentioned features (Laue oscillations, superlattice satellites) are strongly altered. The curve belonging to 2-75 appears to have two main peaks. Since this sample has only one bilayer repetition, it is likely that these two peaks correspond to two Fe-V lattices, one below and one above the Co layer. The intensity of Laue oscillations and satellites with respect to the main peak(s) decreased, compared to

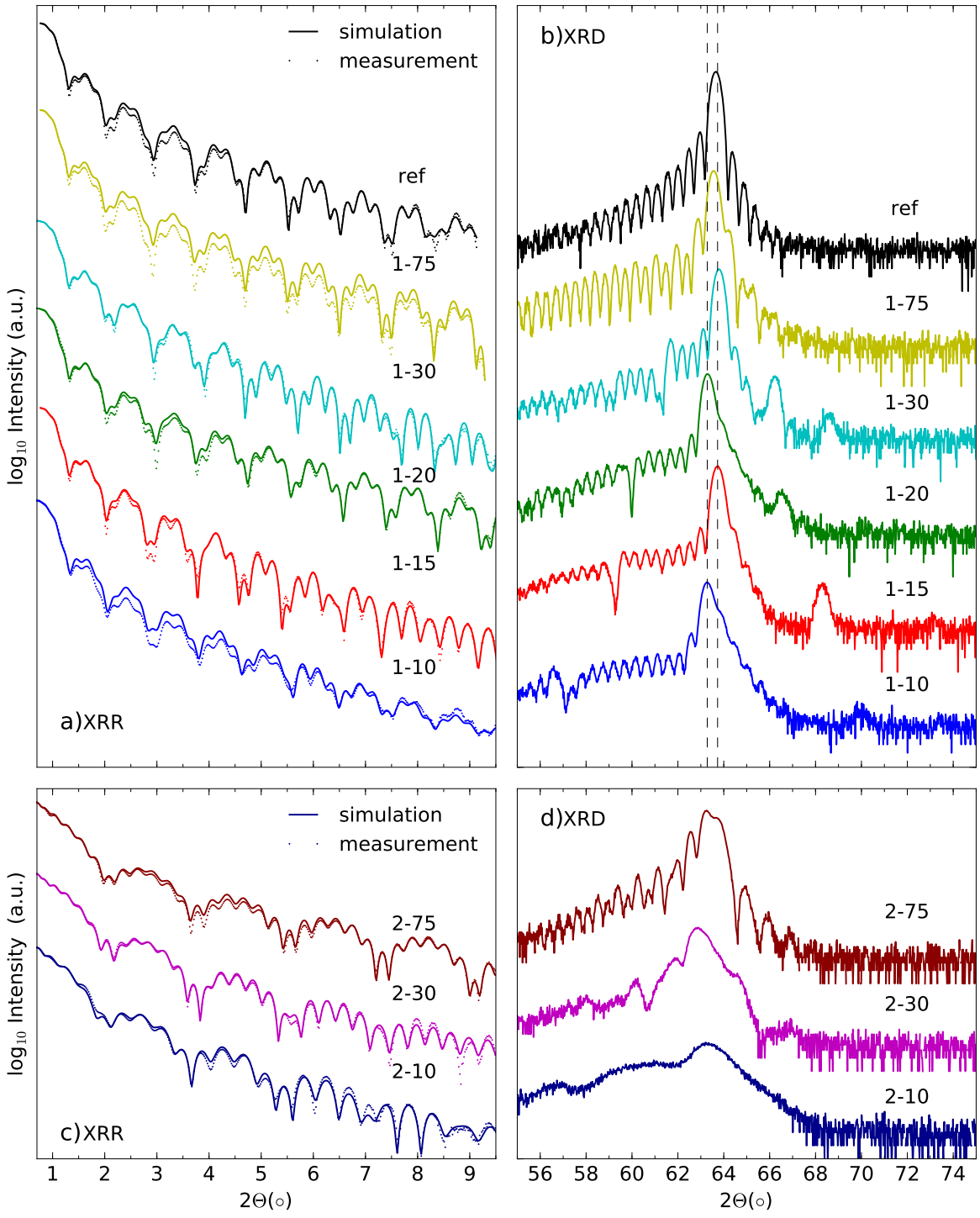

Figure 3.1: *a) Measured and simulated XRR patterns of the superlattices, b) measured XRD patterns around the (002) peak of the superlattices (the dashed drop-lines are used to indicate that the peak positions of most samples group around two values, corresponding to different strain states of the lattices), c) measured and simulated XRR patterns of the multilayers, and d) measured XRD patterns around the (002) peak of the multilayers.*

the scans in Figure 3.1 b). This decrease progresses in the scans of 2-30 and 2-10. It can further be observed that the main peak is significantly broadened in these scans, which suggests a distribution of lattice plane spacings rather than a specific value, or that the coherence length of the crystal is shorter. The lack of typical superlattice characteristics is a consequence of lost coherency as a result of crystal lattice relaxation. It appears that embedding two ML of Co in an Fe-V lattice causes a large degree of relaxation; on the contrary, it is possible to epitaxially include one ML of Co with very little relaxation. Accordingly, the $Co_n/(Fe_{31}V_{69})_m$ films with n=1 are fully coherent superlattices. The n=2 series, on the other hand, will be referred to as multilayers in the following.

We employed XRR to obtain precise values for all relevant thicknesses, as well as an assessment of the interface roughnesses. Total and bilayer thicknesses are documented in Table 3.1. XRR scans are shown in Figure 3.1 a) and c) for the films with one and two ML Co per bilayer, respectively. The simulated curves are in very good agreement with the experimental data; especially, regarding the reproduction of Kiessig fringes. Since it is the character of these interference patterns that corresponds to the layer thicknesses in the samples, we can be confident that our model yields the correct thickness values. The reliability of the fit is supported by XRD data for the bilayer thickness, extracted from the superlattice satellite spacings. The measured values agree excellently with XRR bilayer thicknesses with an average deviation of only 1.7%. The sharp contours and minor decay of the fringes over a large angular range suggest little uncorrelated interface roughness. For some samples, there are discrepancies with respect to the intensity of measured and simulated curves. This might have several origins: sample curvature effects, varying layer densities, correlated roughness resulting from traversing atomic steps, or the fact that our model constrains all interface roughnesses within the superlattice stack to have the same value. However, since, in this case, the intensity variation does not affect the shape of Kiessig fringes, we conclude that layer thicknesses exhibit precisely the intended values and uncorrelated interface roughnesses are low.

3.2 Magnetic properties

We used longitudinal MOKE to investigate the in-plane magnetisation as a function of temperature. As the Co layer density is the varying variable in this study, it is important to provide a reference of the epitaxial Fe-V alloy lattices without any Co. According to the theory of critical phenomena, around a second order phase transition from ferro- to paramagnetism, the spontaneous magnetisation decreases with increasing temperature and can be described by a power law: $M(T) = M_0(1 - T/T_c)^{\beta}$ [30], where M_0 is the spontaneous magnetisation at zero temperature and T_c is the magnetic ordering temperature. The remanent magnetisation, M_r, (taken as the experimental equivalent of the spontaneous magnetisation) of the reference as a function of temperature and the corresponding power law fit are shown in Figure 3.2. The tail of M_r extending beyond T_c, which is frequently observed in numerous thin film studies [2, 31–34], is attributed to structural and compositional inhomogeneities. Matching T_c from the fit (63.8 K) to data from Mustaffa et al. [35] yields an alloy composition of $Fe_{31}V_{69}$ after the deposition series, which corresponds to the value of 31.1% Fe given by the nominal growth rates. A comparison of references from before and after the

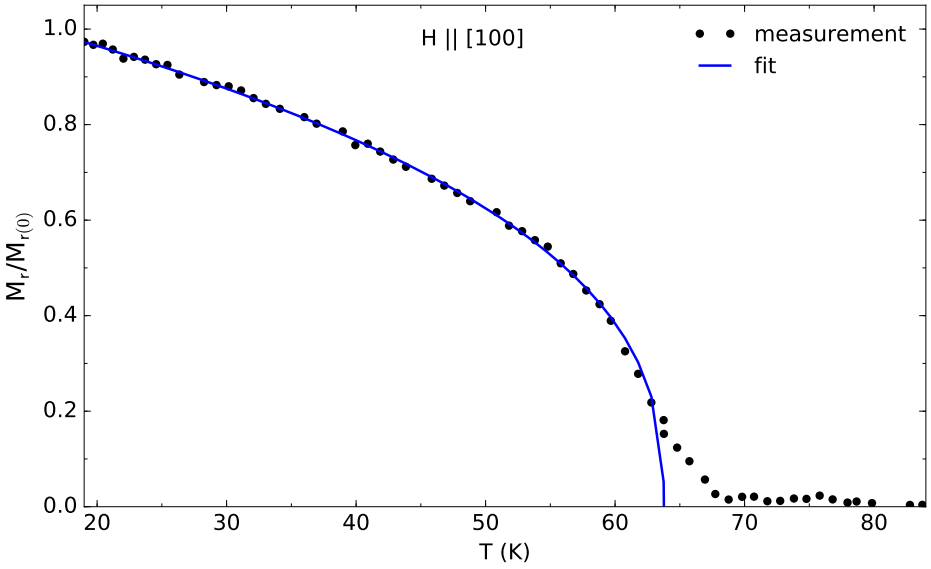

Figure 3.2: *Normalised remanent magnetisation $M_r/M_{r(0)}$ vs. temperature T with field H || [100] of the $Fe_{31}V_{69}$ reference alloy.*

deposition series shows an increase of Fe concentration by only about 0.2%. The fitted coefficient β=0.375(6) corresponds to a 3D Heisenberg universality class [1]. Thin film typical shape anisotropy directs the magnetic moment in-plane and there is no indication for an out-of-plane reorientation. The ratios of maximum field magnetisation vs. remanent magnetisation reveal that [100] is the easy and [110] is the (medium) hard axis of magnetisation (shown later in Figure 3.5), as to be expected for a bcc crystal. For these reasons, it is evident that the Fe-V reference sample undergoes a ferromagnetic phase transition.

Remanent magnetisation, M_r, as a function of temperature of all samples is shown in Figure 3.3. Some of the curves in this figure show a drop in magnetisation followed by an increase before they finally approach zero. A manual inspection of the hysteresis loops yields that this earlier drop is only attributed to noise in the data and that the final approach to zero represents the real behaviour. It is clearly visible that the temperature of zero in-plane magnetisation, $T_{M=0}$, is significantly lowered upon addition of Co layers in the Fe-V lattice. The 2-10 sample does not show any in-plane magnetisation at all. Co has the highest T_c (ca. 1400 K [1]) of all elements; hence, it is highly unlikely that Co layers would actually lower the T_c of the samples in this study. A much more likely explanation is that the magnetic moment in these films is in a canted state, partially pointing out of plane. Such a behaviour is rather unusual for thin films, where the demagnetising factors (N_x, N_y, N_z) can be closely approximated as (0, 0, 1). The resulting shape anisotropy energy in the demagnetising field is

$$E_d = K_{sh} \sin^2(\Theta) \tag{3.1}$$

with

$$K_{sh} = -\frac{1}{2}\mu_0 M^2, \tag{3.2}$$

where Θ is the angle between magnetic moment and film normal, μ_0 is the magnetic constant and M is the total magnetic moment of the film [1]. It favours to align the magnetic moment in the plane of the thin film. In this study, however, there has to be a strong source of perpendicular anisotropy. A perpendicular surface anisotropy, as an

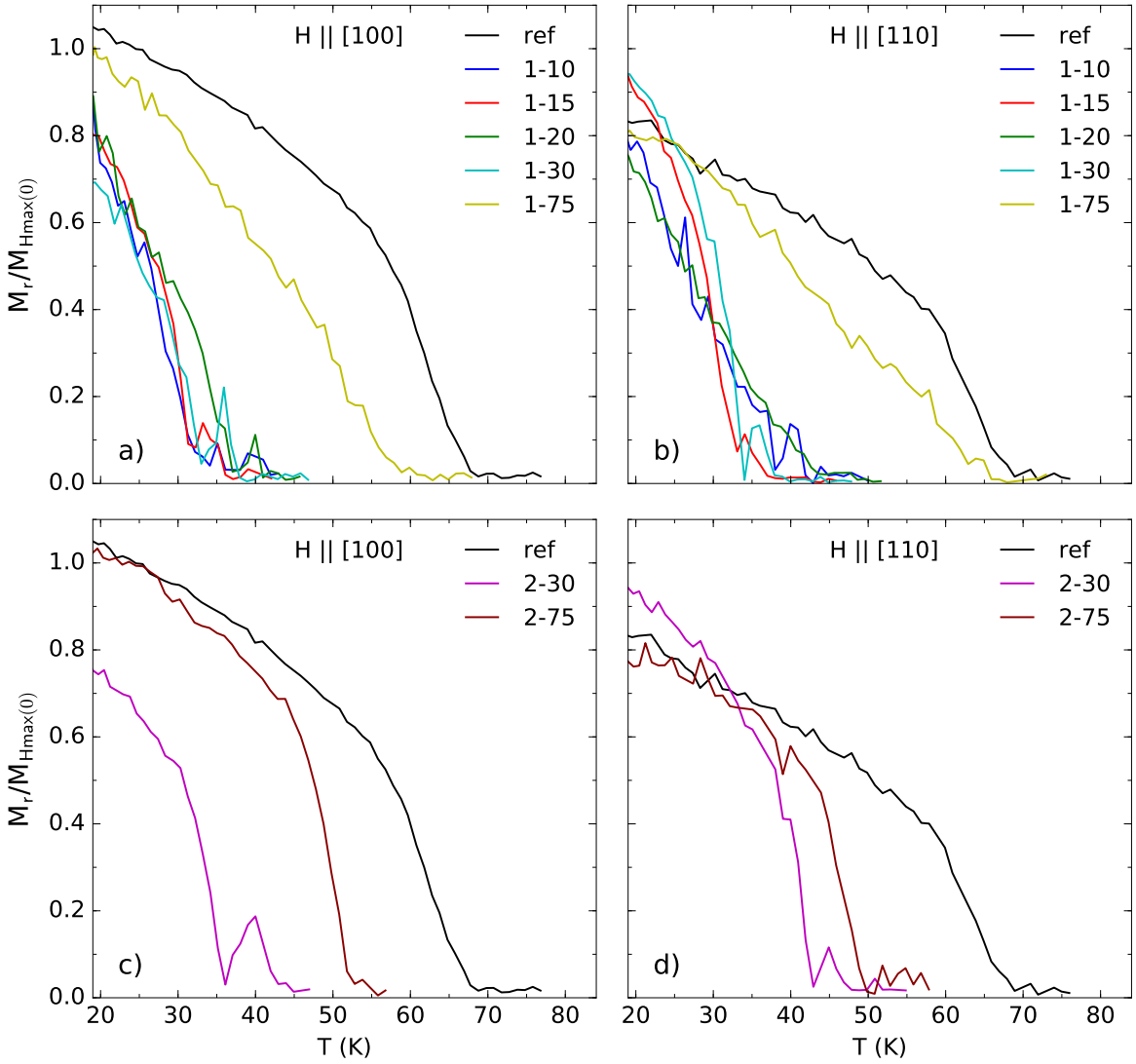

Figure 3.3: *a) Normalised remanent magnetisation $M_r/M_{Hmax(0)}$ vs. temperature T with field H || [100] for superlattices, b) $M_r/M_{Hmax(0)}$ vs. T with H || [110] for superlattices, c) $M_r/M_{Hmax(0)}$ vs. T with H || [100] for multilayers, and d) $M_r/M_{Hmax(0)}$ vs. T with H || [110] for multilayers.*

effect resulting from symmetry break at the surface, was first described by Néel [8]. The energy contribution of the surface anisotropy can be expressed as

$$E_s = -K_s \cos^2(\Theta) + K_{s,p} \sin^2(\Theta) \cos^2(\phi), \tag{3.3}$$

where ϕ is an azimuthal angle. The second term corresponds to an in-plane surface anisotropy which can be neglected for the high symmetry (001) plane. The first term favours to align the moment perpendicular for positive values of K_s [36]. This concept equally applies to interfaces: a break of symmetry leads to a localisation of orbitals and band narrowing along the interface normal, which in turn gives rise to an elevated spin imbalance due to a higher density of states (DOS) at the Fermi level. Furthermore, electronic hybridisation between different interface atoms changes the magnitude of the orbital component of the magnetic moment perpendicular to the interface [36]. Naturally, changes in the unit cell volume resulting from strain have an influence on the DOS, as well, and thereby, can amplify or weaken interface anisotropy.

As mentioned in the Introduction (Ch. 1), perpendicular anisotropy originating from Co layers has been observed in various layered material systems. In most of these studies [9–14, 16–18, 20], the authors observe an onset of perpendicular orientation of the magnetic moment below certain Co layer thicknesses t_{Co} and a $1/t_{Co}$ dependence of its magnitude. This behaviour is consistent with a competition of anisotropies which will be discussed further below. Beside a break of symmetry, the authors discuss other influences on interface anisotropy, such as magneto-crystalline anisotropy contributions K_{mc}, interface smoothness and inter-mixing, and especially strain. In a computational study, Kyuno et al. [15] show that the effect of in-plane tensile strain on the electronic hybridisation significantly enhances perpendicular anisotropy. The magneto-elastic anisotropy, resulting from strain, can be written as

$$K_{me} = \frac{3}{2}\lambda\sigma, \tag{3.4}$$

where λ and σ are magnetrostriction and stress, respectively [1]. Considering all contributions to anisotropy, the effective anisotropy is

$$K_{eff} = K_{mc} + K_{me} + K_s + K_{sh}. \tag{3.5}$$

The two competing terms of interface K_s and shape K_{sh} anisotropy scale with the number of interfaces and the total magnetic moment, respectively. This competition is directly observable in the in-plane magnetisation decrease in Figure 3.3. With increasing temperature, magnetic excitations reduce the magnetic moment and thereby the contribution to the shape anisotropy. Accordingly, the in-plane projection of the moment decreases until the temperature of zero in-plane magnetisation, $T_{M=0}$, where the out-of-plane reorientation is completed. The 2-10 sample's interface anisotropy is so dominant that it does not show any in-plane projection. $T_{M=0}$ are displayed in Figure 3.4. It is noticeable that $T_{M=0}$ does not decrease significantly with increasing number of interfaces, even though the total film thickness is kept roughly constant between 200-225 Å. The contribution to K_{sh}, which compensates K_s, has to originate from the additional Co layers. Hence, the Co atoms have to carry considerably more moment than the Fe-V atoms.

The previously reported $1/t_{Co}$ dependence of the interface anisotropy strength cannot be confirmed in the one ML limit; $T_{M=0}$ is inversely proportional to the interface anisotropy strength, and the $T_{M=0}$ of 1-75 is higher than that of 2-75. Also, a plot of all $T_{M=0}$ as a function of $1/\Lambda$ (not shown here) does not display a linear or even

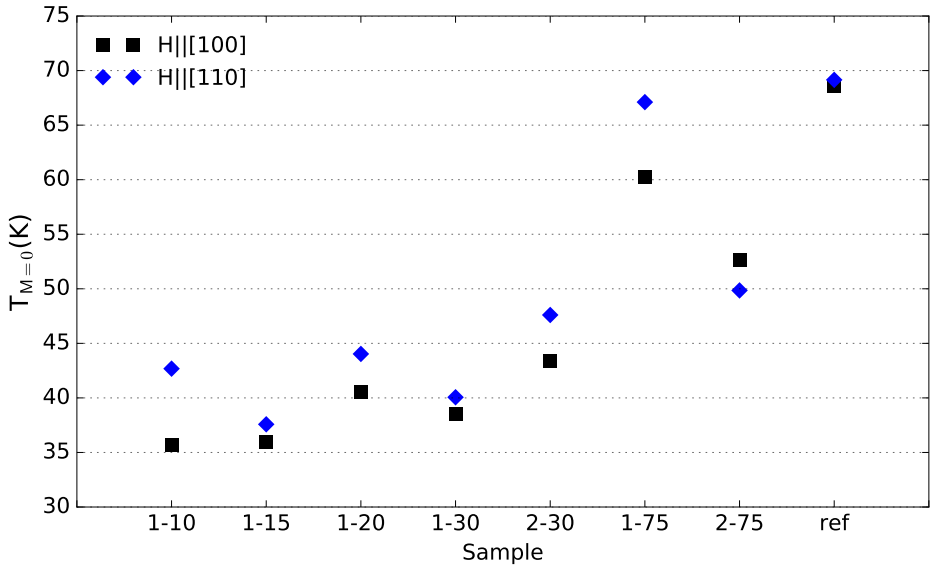

Figure 3.4: *Temperatures of zero in-plane magnetisation $T_{M=0}$.*

monotonous dependence. The strain dependence of the interface anisotropy, which was discussed earlier, might play a role in this study, too. Specimens 1-10, 1-20, and 1-75 have higher out-of-plane lattice parameters than 1-15, 1-30, and the reference (cf. Table 3.1). For these samples, the in-plane magnetisation decrease with increasing temperature differs in shape, particularly || [110]. $T_{M=0}$ || [100] is almost always lower than || [110], but the differences are relatively large for these samples. Though, we cannot explain the effect of strain in our samples more precisely, there seems to be a correlation between the strain state of the crystal lattice and the strength of interface anisotropy that determines the in-plane projection of the magnetic moment, at least along [110].

A comparison of the ratios between remanent magnetisation and maximum field magnetisation, M_r/M_{Hmax}, can yield inferences about the magneto-crystalline anisotropy. M_r/M_{Hmax} as a function of temperature are shown in Figure 3.5 for both H || [100] and H || [110]. As addressed before, for a bcc crystal, the easy axis of magnetisation lies along a $\langle 100 \rangle$ direction. This would ideally result in M_r/M_{Hmax} of 1 and $\sqrt{2}^{-1}$ along [100] and [110], respectively, assuming saturation at H_{max}. Thus, a canted magnetic moment, pointing partially out-of-plane, should still have a larger projection onto [100] than onto [110]. While the reference and n-75 follow these expectations, 1-15 and n-30 reverse it. 1-10 and 1-20 also have lower than expected values along [100]. Since the coordination of atoms is not changed in these samples, an apparent reversal of the magneto-crystalline easy axis is unexpected. It is known that atomic steps in thin films can cause a uni-axial anisotropy parallel to the step edge. Kawakami et al. [37, 38] have shown that hysteresis loops split when field is applied perpendicular to atomic steps. While we observe such splitting in one of the reference films, it is not evident in the samples concerned of the apparent reversal. Therefore, atomic steps can only provide a highly speculative explanation for the observed phenomenon.

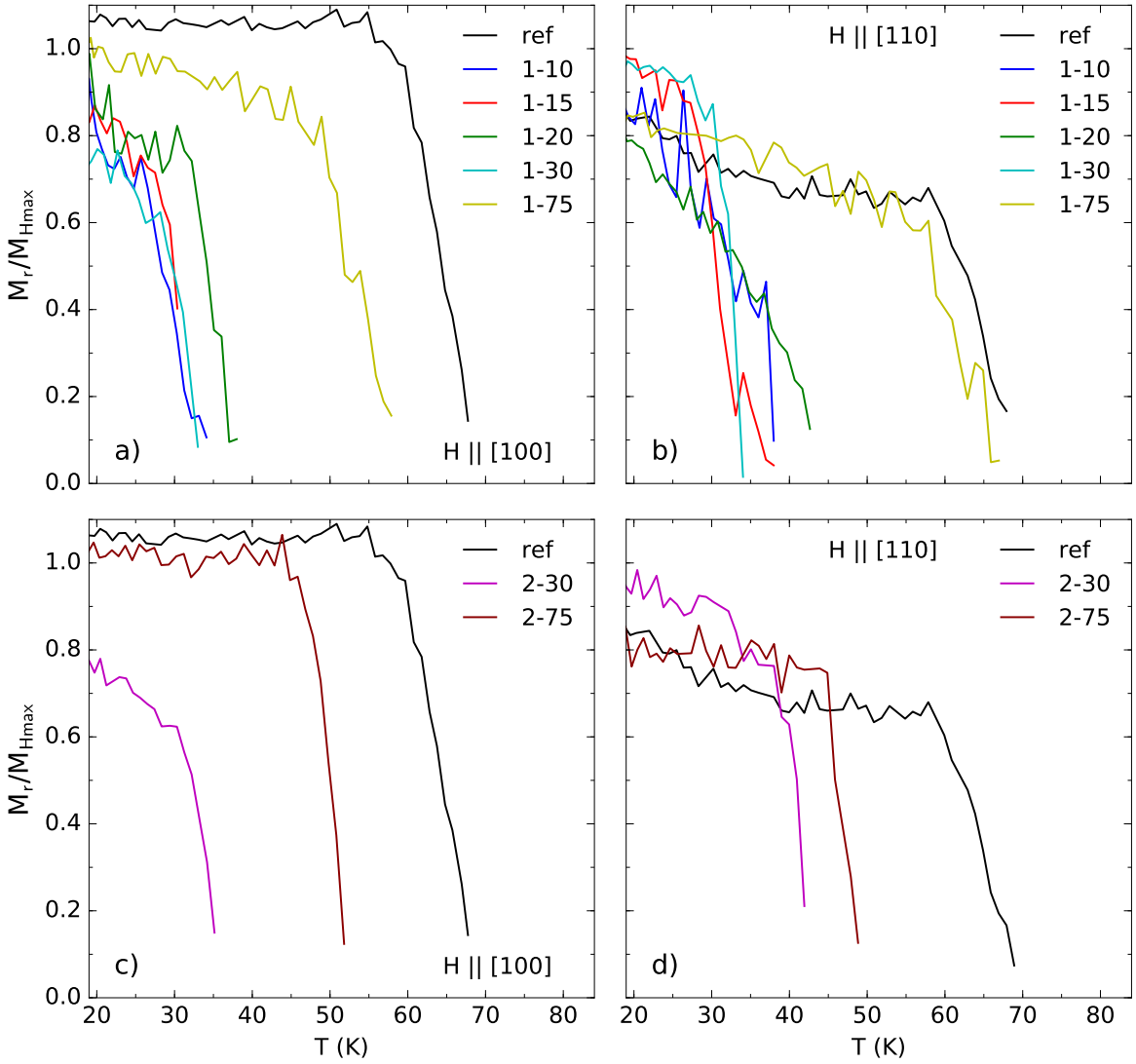

Figure 3.5: *a) Ratio between remanent magnetisation and maximum field magnetisation M_r/M_{Hmax} vs. temperature T with field H || [100] for superlattices, b) M_r/M_{Hmax} vs. T with H || [110] for superlattices, c) M_r/M_{Hmax} vs. T with H || [100] for multilayers, and d)M_r/M_{Hmax} vs. T with H || [110] for multilayers.*

4. Conclusion

We have studied the effect of varying Co layer density in $Co/Fe_{31}V_{69}$ superlattices. For this purpose, $Co_n/(Fe_{31}V_{69})_m$ (n=(0,1,2) ML, m=(10, 15, 20, 30, 75) ML) thin films were epitaxially deposited on MgO using DC magnetron sputtering. Structural characterisation via XRD and XRR reveals that the n=1 samples are fully coherent superlattices with low interface roughness, whereas the n=2 films are partially relaxed. The in-plane remanent magnetisation as a function of temperature was measured with longitudinal MOKE. Upon addition of Co layers into the Fe-V alloy the temperature of zero in-plane magnetisation $T_{M=0}$ is significantly reduced, with respect to the Fe-V alloy reference. This serves as an indicator for a reorientation of the magnetic moment in the out-of-plane direction. The reorientation is caused by a perpendicular anisotropy contribution, originating from the Co interfaces, which is in competition with the thin film typical shape anisotropy. Secondary magneto-crystalline and magneto-elastic contributions to the effective anisotropy appear to also have an influence on the projections of the magnetic moment. We have shown that the degree of reorientation primarily depends on the total magnetic moment of the sample, as well as on the amount of interfaces. Consequently, the process is tunable by temperature, Co layer density, and saturation moment (composition) of the Fe-V alloy.

5. Outlook

The degrees of tunability make Co/Fe-V superlattices an interesting candidate for magneto-electronic devices, but many insights are still missing. We used a longitudinal MOKE setup which only provided a relative measure of the in-plane magnetisation at external fields below saturation of the samples. However, to determine actual functional dependencies, it requires absolute values of the magnetic moment for both in-plane and out-of-plane hysteresis loops that go up to saturation. Therefore, high-field in-plane and out-of-plane measurements via superconducting quantum interference device (SQUID) or vibrating sample magnetometer (VSM) will be performed. The effective anisotropy can be extracted from the area between polar and longitudinal hysteresis loops [9, 10, 14, 17, 18]. Shape anisotropy can be calculated from the absolute moment. Assuming that the contribution of magneto-crystalline anisotropy does not change between the in-plane and out-of-plane ⟨100⟩ directions and neglecting magneto-elastic contributions, the interface anisotropy can be directly obtained.

It would also be valuable to obtain better understanding of strain-induced anisotropy in this material system. It is, however, extremely difficult to precisely control strain experimentally and it would require changing other parameters as well; the different contributions to effective anisotropy would be hard to isolate. In this case, an *ab initio* computational study (cf. Kyuno et al. [15]) would be suitable for observing how a change of unit cell volume effects the electronic structure.

As pointed out in the Introduction (Ch. 1), Co δ-doped superlattices represent well-suited samples for studying the magnetic double proximity effect. Performing the measurements suggested above as a function of temperature allows to study the long-range interactions (as done for the Fe-V alloy reference in (3.2)). This might show how the magnetic proximity effect stabilises magnetic ordering over larger temperature ranges and distances. To improve the understanding of the double proximity effect even further, it is necessary to apply element specific techniques that yield magnetic

moments of the different atomic species, and thereby, not only effective but actual critical power law exponents. Comparing these exponents for different Co layer densities can reveal changes in the systems' dimensionality [30]. This, in turn, will show if an indirect coupling of the delta-layers takes place at certain layer spacings. Such additional understanding provides even more flexibility for tailoring the properties of these complex material systems and pave the way towards exciting new applications of magnetic thin films.

6. Acknowledgement

Special thanks goes to Heikki Palonen and Björgvin Hjörvarsson for supervising this project, as well as to Maciej Kaplan, Agnė Čiučiulkaitė, and the whole materials physics division for helpful discussions. Financial support by the Swedish research council (VR) is acknowledged.

References

[1] J. M. D. Coey. *Magnetism and magnetic materials*. Cambridge University Press, 2010. ISBN 1139486926.

[2] F. Huang, M. T. Kief, G. J. Mankey, and R. F. Willis. Magnetism in the few-monolayers limit: A surface magneto-optic kerr-effect study of the magnetic behavior of ultrathin films of Co, Ni, and Co-Ni alloys on Cu(100) and Cu(111). *Physical Review B*, 49:3962–3971, 1994. doi:10.1103/PhysRevB.49.3962.

[3] A. Taroni and B. Hjörvarsson. Influence of the range of interactions in thin magnetic structures. *The European Physical Journal B*, 77(3):367–371, 2010. doi:10.1140/epjb/e2010-00266-3.

[4] P. K. Manna and S. M. Yusuf. Two interface effects: Exchange bias and magnetic proximity. *Physics Reports*, 535(2):61 – 99, 2014. doi:10.1016/j.physrep.2013.10.002.

[5] O. Rader, E. Vescovo, J. Redinger, S. Blügel, C. Carbone, W. Eberhardt, and W. Gudat. Fe-induced magnetization of Pd: The role of modified Pd surface states. *Physical Review Letters*, 72:2247–2250, 1994. doi:10.1103/PhysRevLett.72.2247.

[6] R. Zeller. Large-scale electronic-structure calculations for isolated transition-metal impurities in Palladium. *Modelling and Simulation in Materials Science and Engineering*, 1(4):553, 1993. doi:10.1088/0965-0393/1/4/016.

[7] M. J. Zuckermann. The proximity effect for weak itinerant ferromagnets. *Solid State Communications*, 12(7):745 – 747, 1973. doi:10.1016/0038-1098(73)90327-X.

[8] L. Néel. Anisotropie magnétique superficielle et surstructures d'orientation. *Journal de Physique et Le Radium*, 15(4):225–239, 1954. doi:10.1051/jphysrad:01954001504022500.

[9] P. F. Carcia, A. D. Meinhaldt, and A. Suna. Perpendicular magnetic anisotropy in Pd/Co thin film layered structures. *Applied Physics Letters*, 47(2):178–180, 1985. doi:10.1063/1.96254.

[10] P. F. Carcia. Perpendicular magnetic anisotropy in Pd/Co and Pt/Co thin film layered structures. *Journal of Applied Physics*, 63(10):5066–5073, 1988. doi:10.1063/1.340404.

[11] B. N. Engel, C. D. England, R. A. Van Leeuwen, M. H. Wiedmann, and C. M. Falco. Interface magnetic anisotropy in epitaxial superlattices. *Physical Review Letters*, 67: 1910–1913, 1991. doi:10.1103/PhysRevLett.67.1910.

[12] R. H. Victora and J. M. MacLaren. Theory of magnetic interface anisotropy. *Physical Review B*, 47:11583–11586, 1993. doi:10.1103/PhysRevB.47.11583.

[13] F. J. A. den Broeder, W. Hoving, and P. J. H. Bloemen. Magnetic anisotropy of multilayers. *Journal of Magnetism and Magnetic Materials*, 93:562 – 570, 1991. doi:10.1016/0304-8853(91)90404-X.

[14] H. J. G. Draaisma, W. J. M. de Jonge, and F. J. A. den Broeder. Magnetic interface anisotropy in Pd/Co and Pd/Fe multilayers. *Journal of Magnetism and Magnetic Materials*, 66(3):351 – 355, 1987. doi:10.1016/0304-8853(87)90169-7.

[15] K. Kyuno, J.-G. Ha, R. Yamamoto, and S. Asano. Magnetoelastic contribution to the interface anisotropy of Pd/Co metallic multilayers. *Physical Review B*, 54: 1092–1099, 1996. doi:10.1103/PhysRevB.54.1092.

[16] F. J. A. den Broeder, D. Kuiper, A. P. van de Mosselaer, and W. Hoving. Perpendicular magnetic anisotropy of Co-Au multilayers induced by interface sharpening. *Physical Review B*, 60:2769–2772, 1988. doi:10.1103/PhysRevLett.60.2769.

[17] C. H. Lee, H. He, F. J. Lamelas, W. Vavra, C. Uher, and R. Clarke. Magnetic anisotropy in epitaxial Co superlattices. *Physical Review B*, 42:1066–1069, 1990. doi:10.1103/PhysRevB.42.1066.

[18] Th. Zeidler, F. Schreiber, H. Zabel, W. Donner, and N. Metoki. Reorientational transition of the magnetic anisotropy in Co/Cr(001) superlattices. *Physical Review B*, 53:3256–3262, 1996. doi:10.1103/PhysRevB.53.3256.

[19] G. H. O. Daalderop, P. J. Kelly, and F. J. A. den Broeder. Prediction and confirmation of perpendicular magnetic anisotropy in Co/Ni multilayers. *Physical Review Letters*, 68:682–685, 1992. doi:10.1103/PhysRevLett.68.682.

[20] F. J. A. den Broeder, E. Janssen, W. Hoving, and W. B. Zeper. Perpendicular magnetic anisotropy and coercivity of Co/Ni multilayers. *IEEE Transactions on Magnetics*, 28(5):2760–2765, 1992. doi:10.1109/20.179619.

[21] S. Mizukami, X. Zhang, T. Kubota, H. Naganuma, M. Oogane, Y. Ando,

and T. Miyazaki. Gilbert damping in Ni/Co multilayer films exhibiting large perpendicular anisotropy. *Applied Physics Express*, 4(1):013005, 2011. doi:10.1143/APEX.4.013005.

[22] S. Fukami, T. Suzuki, H. Tanigawa, N. Ohshima, and N. Ishiwata. Stack structure dependence of Co/Ni multilayer for current-induced domain wall motion. *Applied Physics Express*, 3(11):113002, 2010. doi:10.1143/APEX.3.113002.

[23] M. Björck and G. Andersson. *GenX*: an extensible X-ray reflectivity refinement program utilizing differential evolution. *Journal of Applied Crystallography*, 40(6): 1174–1178, 2007. doi:10.1107/S0021889807045086.

[24] K. Levenberg. A method for the solution of certain non-linear problems in least squares. *Quarterly of Applied Mathematics*, 2(2):164–168, 1944.

[25] D. W. Marquardt. An algorithm for least-squares estimation of nonlinear parameters. *Journal of the Society for Industrial and Applied Mathematics*, 11(2):431–441, 1963. doi:10.1137/0111030.

[26] M. Wojdyr. *Fityk*: a general-purpose peak fitting program. *Journal of Applied Crystallography*, 43(5 Part 1):1126–1128, 2010. doi:10.1107/S0021889810030499.

[27] H. H. Ku. Notes on the use of propagation of error formulas. *Journal of Research of the National Bureau of Standards*, 70(4):263, 1966. doi:10.6028/jres.070C.025.

[28] S. Sasaki, K. Fujino, and Y. Takuchi. X-ray determination of electron-density distributions in oxides, MgO, MnO, CoO, and NiO, and atomic scattering factors of their constituent atoms. *Proceedings of the Japan Academy, Series B*, 55(2):43–48, 1979. doi:10.2183/pjab.55.43.

[29] P. F. Fewster. *X-ray Scattering from Semiconductors*. World Scientific, 2003. ISBN 1860943608.

[30] H. E. Stanley. *Introduction to phase transitions and critical phenomena*, volume 1. Oxford University Press, 1987. ISBN 0195053168.

[31] M. Pärnaste, M. van Kampen, R. Brucas, and B. Hjörvarsson. Temperature-dependent magnetization and susceptibility of Fe_n/V_7 superlattices. *Physical Review B*, 71:104426, 2005. doi:10.1103/PhysRevB.71.104426.

[32] E. Th. Papaioannou, V. Kapaklis, A. Taroni, M. Marcellini, and B. Hjörvarsson.

Dimensionality and confinement effects in δ-doped Pd(Fe) layers. *Journal of Physics: Condensed Matter*, 22(23):236004, 2010. doi:10.1088/0953-8984/22/23/236004.

[33] M. Ahlberg, M. Marcellini, G. Taroni, A.and Andersson, M. Wolff, and B. Hjörvarsson. Influence of boundaries on magnetic ordering in Fe/V superlattices. *Physical Review B*, 81:214429, 2010. doi:10.1103/PhysRevB.81.214429.

[34] M. Ahlberg, P. Korelis, G. Andersson, and B. Hjörvarsson. Effect of ferromagnetic proximity on critical behavior. *Physical Review B*, 85:224425, 2012. doi:10.1103/PhysRevB.85.224425.

[35] A. Mustaffa and D. A. Read. Magnetic properties of ferromagnetic VFe alloys near the critical concentration for ferromagnetism. *Journal of Magnetism and Magnetic Materials*, 5(4):349 – 352, 1977. doi:10.1016/0304-8853(77)90147-0.

[36] C. A. F. Vaz, J. A. C. Bland, and G. Lauhoff. Magnetism in ultrathin film structures. *Reports on Progress in Physics*, 71(5):056501, 2008. doi:10.1088/0034-4885/71/5/056501.

[37] R. K. Kawakami, E. J. Escorcia-Aparicio, and Z. Q. Qiu. Symmetry-induced magnetic anisotropy in Fe films grown on stepped Ag(001). *Physical Review Letters*, 77:2570–2573, 1996. doi:10.1103/PhysRevLett.77.2570.

[38] R. K. Kawakami, M. O. Bowen, H. J. Choi, E. J. Escorcia-Aparicio, and Z. Q. Qiu. Effect of atomic steps on the magnetic anisotropy in vicinal Co/Cu(001). *Physical Review B*, 58:R5924–R5927, 1998. doi:10.1103/PhysRevB.58.R5924.